

ADCT-402, a PBD dimer-containing antibody drug conjugate targeting CD19-expressing malignancies

Francesca Zammarchi¹, Simon Corbett^{2,3}, Lauren Adams², Peter C Tyrer², Konstantinos Kiakos³, Narinder Janghra⁴, Teresa Marafioti⁴, Charles E Britten¹, Carin EG Havenith¹, Simon Chivers¹, Francois D'Hooge², David G Williams², Arnaud Tiberghien², Philip W Howard², John A Hartley^{1,2,3}, and Patrick H van Berkel¹.

¹ADC Therapeutics (UK) Limited, QMB Innovation Centre, 42 New Road, London, E1 2AX, UK

²Spirogen/Medimmune Ltd, QMB Innovation Centre, 42 New Road, London, E1 2AX, UK

³Cancer Research UK Drug DNA Interactions Research Group, UCL Cancer Institute, 72 Huntley Street, London, WC1E 6BT, UK

⁴Department of Pathology, UCL Cancer Institute, 72 Huntley Street, London, WC1E 6BT, UK

Prior Presentation: Partially presented in poster forms at the 57th Annual Meeting of the American Society of Hematology, Orlando, FL, December 7, 2015 and at the American Association for Cancer Research Annual Meeting 2017, Washington, DC, April 2, 2017.

Short title: ADCT-402 targets CD19-expressing B-cell malignancies

Corresponding author:

Francesca Zammarchi, ADC Therapeutics (UK) Limited, QMB Innovation Centre, 42 New Road, London, E1 2AX, UK; francesca.zammarchi@adcttherapeutics.com

Tel. +44 (0) 2030214653

Text word count: 3985

Figures: 7

Tables: 1

Key points:

- ADCT-402 is a novel CD19-targeted ADC delivering SG3199, a highly cytotoxic DNA minor groove interstrand cross-linking PBD dimer warhead
- ADCT-402 has potent and selective anti-tumor activity against CD19-expressing haematological malignancies warranting clinical development

ABSTRACT

Human CD19 antigen is a 95-kDa type I membrane glycoprotein in the immunoglobulin superfamily whose expression is limited to the various stages of B-cell development and differentiation and is maintained in the majority of B-cell malignancies, including leukemias and non-Hodgkin lymphomas of B-cell origin. Coupled with its differential and favourable expression profile, CD19 has rapid internalization kinetics and it is not shed into the circulation, making it an ideal target for the development of antibody-drug conjugates (ADCs) to treat B-cell malignancies.

ADCT-402 (loncastuximab tesirine) is a novel CD19-targeted ADC delivering SG3199, a highly cytotoxic DNA minor groove interstrand cross-linking pyrrolobenzodiazepine (PBD) dimer warhead. It showed potent and highly targeted in vitro cytotoxicity in CD19-expressing human cell lines. ADCT-402 was specifically bound, internalized and trafficked to lysosomes in CD19-expressing cells and following release of warhead, resulted in formation of DNA cross-links which persisted for 36 h. Bystander killing of CD19-negative cells by ADCT-402 was also observed. In vivo, single doses of ADCT-402 resulted in highly potent, dose-dependent anti-tumor activity in several subcutaneous and disseminated human tumor models with marked superiority to comparator ADCs delivering tubulin inhibitors. Dose-dependent DNA cross-links and γ -H2AX DNA damage response were measured in tumors by 24 h after single dose administration, while matched PBMCs showed no evidence of DNA

damage. Pharmacokinetic analysis in rat and cynomolgus monkey showed excellent stability and tolerability of ADCT-402 in vivo.

Together, these impressive data were used to support the clinical testing of this novel ADC in patients with CD19-expressing B-cell malignancies.

INTRODUCTION

Human CD19 antigen is a 95-kDa type I membrane glycoprotein belonging to the immunoglobulin superfamily¹. In normal human tissue, CD19 expression is restricted to the various stages of B-cell development and differentiation (except hematological stem cells and plasma cells)^{2,3} and its expression is maintained in the majority of B-cell malignancies, including leukemias and non-Hodgkin lymphomas (NHL) of B-cell origin⁴.

Because of its widespread expression, CD19 is an attractive therapeutic target and several antibody-based therapies are in clinical development⁵. A bispecific scFv anti-CD19/anti-CD3 bispecific T-cell engager blinatumomab (Blinicyto™) is approved for the treatment of second-line Philadelphia chromosome-negative relapsed or refractory (R/R) acute lymphoblastic leukemia⁶. CD19 also remains the most investigated target for CAR T-cell therapy⁷.

CD19 has rapid internalization kinetics^{8,9} and it is not shed into the circulation¹⁰. These features, coupled with its differential and favourable expression profile, make CD19 an ideal target for the development of antibody-drug conjugates (ADCs) to treat B-cell malignancies. Indeed, anti-CD19 auristatin containing ADC denintuzumab mafodotin (SGN-CD19A)¹¹ and maytansinoid-containing coltuximab ravtansine (SAR3419)¹² have been investigated in the clinic.

As an alternative to the delivery of tubulin binding-based warheads, novel ADCs delivering highly cytotoxic pyrrolobenzodiazepine (PBD) dimers have been developed¹³⁻¹⁵. PBD dimers are a class of exquisitely potent DNA minor groove interstrand cross-linking agents¹⁶; one of which, SG2000 (SJG-136) has shown activity against both solid tumor and haematological malignancies^{17,18}. Advantages over ADCs employing other warheads including tubulin inhibitors (e.g. auristatins and maytansinoids), DNA cleavage agents (e.g. calicheamicin) and classical chemotherapeutics, include the ability to target low copy number antigens and tumor-initiating cells¹⁴, and to exploit low drug-antibody ratios (DARs). Because of their novel

mechanism of action, PBD-containing ADCs are active in tumors inherently resistant to other warhead types and against multidrug-resistant cancers¹³.

PBD dimer SG3199¹⁹ is the released warhead component of the ADC payload tesirine (SG3249)²⁰, currently being evaluated clinically in several ADCs including ADCT-301, ADCT-502, MEDI3726 and rovalpituzumab tesirine (Rova-T) for which Phase I data in small cell lung cancer has been reported²¹, and which is currently in several Phase II and Phase III studies.

Here, we report the preclinical evaluation of the novel anti-CD19 ADC ADCT-402 (loncastuximab tesirine) containing the PBD dimer payload tesirine. On the basis of these impressive pre-clinical data, this agent is currently being evaluated in Phase I studies of both R/R NHL and R/R B-ALL.

METHODS

Synthesis of ADCs

RB4v1.2 antibody was conjugated to tesirine essentially as previously described¹⁵. The ADC was formulated in 30 mM histidine, 200 mM sorbitol, 0.02% Tween-20, pH 6.0. The solution was filtered (0.22 µm) and stored at -70°C.

ADCs RB4v1.2-DM4 and hBU12-mc-MMAF were generated by ConcorTis (San Diego, USA) as described in ²² and in patent US 8,242,252 B2, respectively.

Characterisation of ADCT-402 by SEC, HIC and RPLC

Characterisation of synthesised ADCT-402 was performed by size exclusion chromatography (SEC), hydrophobic interaction chromatography (HIC) and reduced reverse phase liquid chromatography (RPLC), as previously described¹⁵.

Human cell lines

The source of cell lines used in this study along with cell growth media are shown in Supplementary Table S1.

CD19 cell surface density

Cell surface CD19 density was determined using Bangs Laboratory Quantum Simply Cellular Anti-human IgG beads according to the manufacturer's instructions.

In vitro cell killing and bystander assay

Cell lines were incubated in growth medium with serial dilutions of ADCT-402, the isotype control ADC, or the free warhead SG3199 for 5 days at 37 °C in a 5% CO²-gassed, humidified incubator. Cell viability was measured with CellTiter 96® AQueous One Solution Cell Proliferation (Promega) according to manufacturer's instructions. The data were normalised to vehicle-treated cells. IC₅₀ values were determined by using GraphPad software (GraphPad, San Diego, CA). The mean and standard errors of the means of three independent IC₅₀ values were determined.

For the bystander assay, Ramos or NCI-N87 cells were incubated for the indicated time points with ADCT-402. Condition medium was transferred to Karpas-299 cells, incubated for 4 days and cell viability measured.

Internalization studies

Cells were exposed to ADCT-402 for 1 h at 4°C and then incubated at 37°C where appropriate. Following permeabilization of cells using Tween-20 (0.1% v/v in PBS) for 15 min, samples were washed with PBS and centrifuged at 4000 rpm (4°C). Removal of the supernatant was followed by addition of rabbit mAb LAMP-1 (1:400; Cell Signalling) for 1 h on ice. A further wash step was followed by adding both Alexa Fluor 488 goat anti human (1:200; Thermo Fisher) for detecting the ADC, and Alexa Fluor 568 goat anti rabbit (1:200; Thermo Fisher). Both secondary antibody incubations were performed on ice for 60 min. Nuclei were counterstained with Hoescht 33342 (Thermo Fisher), then cytopins of cell

samples were prepared and samples mounted in ProLong Gold anti-fade (Life Tech) and cover-slipped.

In vitro and in vivo cross-linking determination

Quantification of in vitro and in vivo cross-links was done by the single cell gel electrophoresis (comet) assay²³ following the protocol and reagents previously described¹⁵.

Assessment of ADCT-402 efficacy in in vivo models

All animal studies were performed in facilities that are accredited by the Association for Assessment and Accreditation of Laboratory Animal Care (AAALAC), which assures compliance with accepted standards for the care and use of laboratory animals. Ramos, Daudi and WSU-DLCL2 xenografts were established in 8-10-week-old female Fox Chase SCID® (Charles River) by implanting 10^7 cells subcutaneously (s.c.) into their flanks. When group mean tumor volumes reached approximately 116-132 mm³, mice were randomly allocated into groups to receive test agent or vehicle. Each animal was euthanized when its tumor reached the endpoint volume or at study end. The time to endpoint (TTE) for analysis was calculated for each mouse by the following equation:

$$\text{TTE (days)} = ([\log_{10}(\text{endpoint volume} - \text{intercept}^*)] / \text{slope}^*)$$

*of the line obtained by linear regression of a log-transformed tumor growth data set

The logrank test was used to analyze the significance of differences between the TTE values of two groups.

For the disseminated xenografts model, 5×10^6 Ramos cells and 1×10^7 NALM-6 cells were injected IV into the lateral tail vein of 5-7 week old, female Fox Chase SCID® and NOG (NOD.Cg-Prkdcscid Il2rg^{tm1Sug}/JicTac) (Taconic) mice, respectively. Treatment with test compounds was initiated 7 days and 3 days after tumor inoculation in Ramos and NALM-6 models, respectively. The day of death or euthanasia represented the TTE. Animals that did

not reach the endpoint were euthanized at the end of the study, and assigned a TTE value equal to the last study day. The logrank test was employed to determine the significance of the difference between the overall survival experiences (survival curves) of two groups, based on their TTE values.

Immunohistochemistry of tumor xenografts and clinical samples sections

Detection of phospho-histone H2A.X (Cell signalling #2577) and anti-PBD (Mouse monoclonal 14B3-B7; Spirogen) in murine FFPE tissue sections was performed using the Leica Bond Max automated staining platform. In brief, both primary antibodies were applied at 1:50 dilution for 30 min, following antigen retrieval of sections using Epitope retrieval solution 2 (Leica Biosystems). Peroxidase block (3-4% (v/v) H₂O₂) followed primary antibody application and antibody detection was performed using the Bond Polymer refine detection system (Leica Biosystems; DS9800). Detection of human CD19 (Leica NCL-CD19-163) in FFPE tissue sections of murine xenograft and human clinical samples was performed using the Roche BenchMark Ultra staining system. In brief, CD19 primary antibody was applied for 30 min at 1:50 dilution following antigen retrieval of sections using CC1 solution (Ventana) for 60 min and a peroxidase blocking step. Detection of anti-CD19 antibody was performed using the Optiview DAB detection kit (# 760-700).

Human lymphoma and leukaemia cases enrolled in this study (Table 1) were diagnosed according to the criteria of the WHO classification for haematological malignancies²⁴ by an expert haematopathologist (TM) at UCLH. The immunohistochemical investigation was conducted according to the principles of the Helsinki declaration after approval of the internal review board, the National Research Ethics Service, Research Ethics Committee 4 (REC Reference number 09/H0715/64).

Assessment of ADCT-402 pharmacokinetics (PK)

All animal studies were performed at research facilities AAALAC accredited.

Male Crl:CD(SD) rats (Charles River Laboratories, UK) were dosed IV with ADCT-402. Blood was collected from tail veins at specified time points; serum was isolated and stored at -80°C.

Male and female purpose bred Cynomolgus monkeys (*Macaca fascicularis*) were dosed IV with ADCT-402. Blood was collected from vena cephalica antebrachii or vena saphena at specific time points; serum was isolated and stored at -80°C.

In rat and monkey serum, quantification of total antibody and ADC (DAR \geq 1) were determined using optimized ECLIA homogenous formats. Calibration curves, QCs and study samples were diluted and mixed with a biotinylated anti-idiotypic antibody for both the total antibody and ADC measurements (biotinylated anti-PBD antibody for ADC in the monkey) and a Sulfo-tag labelled anti-idiotypic antibody for total antibody and a Sulfo-tag labelled anti-PBD antibody for the ADC (Sulfo-tag labelled anti-idiotypic antibody for ADC in the monkey) to allow complex formation. The complex was added to streptavidin coated MSD plates and, following the addition of read buffer, the plate was read on the MSD QuickPlex Plate Reader (6000 Sector Imager (MSD) for the monkey).

The determination of free SG3199 in cynomolgus monkey serum was performed by LC-MS/MS and used deuterium-labelled SG3199 (SG3199-d10) as internal standard. Isolation of SG3199 (and spiked SG3199-d10) was performed by reduction with cyanoborohydride overnight and followed by off-line solid phase extraction using Oasis HLB 96-well μ Elution Plate, 30 μ m Particle Size. The purified samples were analyzed using an AB Sciex Qtrap 5500 LC-MS/MS system with a Zorbax SB-AQ Rapid Resolution HT (2.1 x 50 mm; 1.8 μ m) column.

The PK analysis was performed using Phoenix WinNonlin Version 6.2 with non-compartmental analysis.

RESULTS

Properties of ADCT-402

ADCT-402 is composed of the humanized IgG1 antibody RB4v1.2²⁵, directed against human CD19, conjugated at interchain cysteines to tesirine using maleimide chemistry. Tesirine consists of a cathepsin-cleavable valine-alanine linker that releases the PBD dimer warhead SG3199²⁰ (Figure 1A). ADCT-402 is 96% monodisperse as determined by SEC (Figure 1B). DAR was determined to be 2.3 by RPLC (Figure 1C) and HIC (Figure 1D).

Selective cytotoxicity of ADCT-402 *in vitro*

The *in vitro* cytotoxicity of ADCT-402 was determined in a panel of eight CD19-expressing and two non-expressing cell lines. IC₅₀ values were plotted against the cell surface CD19 density for each cell line (Figure 2A), where a weak, yet significant negative correlation was observed (r value -0.7, p-value 0.024). In contrast, SG3199, the PBD dimer warhead component of ADCT-402, did not show any relationship between IC₅₀ value and cell surface CD19 (r value -0.44, p-value 0.2), consistent with its non-target nature. Interestingly, the Granta-519 and NALM-6 cell lines, which were the most sensitive to SG3199, also showed the greatest sensitivity to the ADC.

ADCT-402 Mechanism of Action

CD19-expressing Ramos cells exposed to ADCT-402 (1 h at 4 °C) showed prominent cell surface binding (T=0, Figure 3A). On incubation at 37 °C, ADCT-402 showed internalization with some cell membrane labelling still evident at 1 h but also some co-localization with lysosomes. This co-localization increased at 2 and 4 h and no evidence of residual ADC staining was evident at 24 h suggesting complete lysosomal degradation.

DNA interstrand cross-linking was measured using a modification of the single cell gel electrophoresis (comet) assay. Cross-linking was expressed as the percentage decrease in Olive Tail Moment (OTM) compared to control irradiated cells. Following a 2-h exposure of Ramos cells to ADCT-402, the time course of cross-link formation is shown in Figure 3B. Cross-links form after an initial delay, reaching a peak at around 12 h, which persist up to 36 h. In contrast, the free warhead SG3199 reached the peak of cross-linking during the initial 2-h exposure. An equivalent concentration of a non-binding ADC did not show the formation of any cross-links.

Ramos cells were treated with ADCT-402 for 1, 2, or 3 days, before transferring the media onto CD19-negative Karpas-299 cells, and incubating for 96 h. ADCT-402 conditioned medium elicited a bystander effect after 1 day of pre-treatment, as shown by a decrease in percentage survival in the conditioned medium-treated Karpas-299 cells compared to the non-conditioned medium (100% to 86%, Figure 3C, left panel). The effect was even greater after 2 or 3 days of pre-incubation in Ramos cells, as shown by a further decrease in percentage cell survival compared to the non-conditioned medium (80% and 65%, $p = 0.001$). Conversely, conditioned medium from ADCT-402-treated, CD19-negative NCI-N87 cells did not elicit any bystander effect when transferred onto Karpas-299 cells, regardless of pre-incubation time (Figure 3C, right panel).

ADCT-402 In Vivo Efficacy

ADCT-402 demonstrated dose-dependent anti-tumor activity against both s.c. and disseminated tumor models in vivo. In the s.c. Ramos xenograft, a single dose of ADCT-402 at 0.33, 0.66 and 1 mg/kg induced dose-dependent anti-tumor activity and resulted in 5/10 and 10/10 tumor-free survivors (TFS) at the 0.66 and 1 mg/kg doses, respectively, on day 60 (Figure 4A). The resulting Kaplan-Meier survival curves show the dose-dependent extension of survival (log-rank test, $p \leq 0.004$ for each comparison, Supplementary Figure S1A).

In the same Ramos model, ADCT-402 was tested together with the CD19-targeted ADCs delivering maytansinoid (RB4v1.2-DM4, DAR=3.3) or auristatin (hBU12-mc-MMAF, DAR=4.2) warheads. ADCT-402 at a single dose of 1 mg/kg was remarkably superior to both the ADCs delivering tubulin binders at an equivalent single dose (Figure 4B). This superiority was maintained for ADCT-402 at 1 mg/kg even when the comparator ADCs were administered at higher doses with multiple administrations; 3.3 mg/kg, q4dx2 for RB4v1.2-DM4 and 3 mg/kg, q4dx4 for hBU12-mc-MMAF, respectively (Figure 4B). The equivalent warhead amounts administered are given in Table S2 and Kaplan-Meier survival curves are shown in Figure S1B. ADCT-402 administered at 1 mg/kg induced a significant increase in survival compared to both comparator ADCs irrespective of dose level and frequency of administration (log-rank test, $p \leq 0.001$ for each comparison).

In this same model, while a single dose of ADCT-402 at 1 mg/kg gave 10/10 TFS (Figure 4C), fractionating the dose to 0.33 mg/kg given weekly x 3, or every 4 days x 3, did not achieve the same level of efficacy (Figure 4C).

In a disseminated Ramos model, single dose ADCT-402 also showed significant extension of survival in comparison to controls (log-rank test, $p \leq 0.001$, Figure 4D) with 9/10 and 10/10 animals surviving at day 91 for the 0.33 and 1 mg/kg groups, respectively, compared to no survival at day 19 for the vehicle and 1 mg/kg non-target ADC groups.

ADCT-402 also showed dose-dependent activity in the CD19-expressing Daudi xenograft model (Figure 5A). At a single dose of 0.3 mg/kg all the animals achieved complete regression with 7/10 classified as TFS at the end of the study (day 73). Kaplan-Meier survival curves show the dose-dependent extension of survival (log-rank test, $p \leq 0.001$ for each comparison, Figure S2A).

ADCT-402 was less effective at treating the WSU-DLCL2 xenograft model (Figure 5B).

Although a clear dose-response was observed, the highest single dose used (1 mg/kg) only

produced a 30 day tumor growth delay. Yet, ADCT-402 resulted in significant, dose-dependent extension of survival (log-rank test, $p \leq 0.002$ for each comparison, Figure S2B).

In a second disseminated model (NALM-6), ADCT-402 at 0.33 and 1 mg/kg single dose produced a significant increase in survival compared to control ADC (log-rank test, $p \leq 0.001$, Figure 5C). At a dose of 1 mg/kg, 10/10 animals survived 90 days compared to only 21 days for the vehicle treated group.

ADCT-402 Pharmacodynamics

In mice with Ramos s.c. tumors, a single dose of ADCT-402 was administered at 0.3 or 1 mg/kg (Figure S3). Twenty-four h after treatment, excised tumors showed a dose-related increase in staining intensity by an anti-PBD drug-linker antibody and a γ -H2AX antibody (Figure 6A). In contrast, tumors excised from mice treated with a non-targeted ADC, containing the same PBD dimer warhead, at 1 mg/kg did not show increased staining compared to vehicle control animals. CD19 staining remained high and homogeneous in all treatment groups (Figure 6A).

Tumor samples were analysed for formation of DNA interstrand cross-linking and γ -H2AX foci. A significant increase in the level of γ -H2AX foci was observed in tumor cells at both ADCT-402 dose levels (Figure 6B), with no significant increase seen with the non-targeted ADC. DNA interstrand cross-linking in tumor cells, measured as the reduction in OTM, was also significant at both dose levels of ADCT-402 compared to vehicle or non-targeted ADC (Figure 6C). In contrast, no cross-linking was observed in PBMCs samples taken from the same mice (Figure S4). The selective targeting of ADCT-402 to human CD19-expressing tumor cells, resulting in the formation of DNA interstrand cross-links and an associated DNA damage response are therefore confirmed *in vivo*.

ADCT-402 Pharmacokinetics in Rat and Cynomolgus Monkey

Quantitation of total or PBD-conjugated antibody was determined in rat serum following a single administration of 1.5 mg/kg to non-tumor bearing rats (Figure 7A). The half-life for total and PBD-conjugated antibody were 9.9 and 10.4 days, respectively (ADCT-402 does not cross-react with rat CD19) (Table S3), indicating typical IgG1 kinetics and excellent stability *in vivo*.

Quantitation of total antibody, PBD-conjugated antibody and free SG3199 was also determined following administration of 0.6 mg/kg ADCT-402 on days 1 and 22 to cynomolgus monkeys (Figure 7B). The exposure profile of ADCT-402 indicates typical IgG1 kinetics, a 14 day half-life (ADCT-402 does not cross-react with cynomolgus monkey CD19) (Table S3), and excellent stability *in vivo*.

ADCT-402 was well tolerated in the rat and monkey studies with an acceptable safety profile.

DISCUSSION

PBD-based ADCs are becoming established as important next-generation agents in the ADC arena. They exploit a completely different cellular mechanism to the first generation auristatin and maytansinoid tubulin inhibitors, and a different mode of DNA interaction to warheads such as calicheamicin²⁶. Several PBD-containing ADCs have entered early phase clinical trials, falling into two distinct classes based on linker site attachment to the PBD dimer; C2 and N10. ADCT-402 is an example where the PBD warhead SG3199 is connected via its N10 position to a maleimidocaproyl valine- alanine dipeptide linker. This drug linker, tesirine, is the same as that in the clinical stage agents rovalpituzumab tesirine, ADCT-301, ADCT-502 and MEDI3726. As the N10-position imine is involved in covalent binding to DNA, linker attachment at this position produces a prodrug, adding a further level of safety over C2-linked agents. Consequently, attachment at the N10-imine requires a self-immolative linker that becomes completely traceless following cleavage, as found in tesirine.

A CD19-directed ADC employing a first-generation PBD dimer with linker site attachment at the C2 position has recently been described²⁷.

ADCT-402 cytotoxicity showed a weak, yet significant negative linear correlation with cell surface CD19 target expression in a panel of ten hematological cancer cell lines (eight CD19-positive and two CD19-negative). This is in contrast to previously reported data for ADCT-301 and SGN-CD19B, which failed to show a clear relationship between sensitivity and antigen expression level^{15,27}. In the case of ADCT-301, the limited number of CD25-positive cell lines available all had high CD25 expression which may have been above a threshold for accurately determining cytotoxic sensitivity. In this study, all cell lines, including those negative for CD19 expression, were sensitive to the free warhead SG3199, consistent with the non-targeted delivery of the warhead alone. Some differential sensitivity, unrelated to CD19 expression, was observed for SG3199. Notably, the mantle cell lymphoma cell line Granta-519 and acute lymphoblastic leukemia cell line Nalm-6 were the most sensitive to both the ADC and the free warhead. Hematological cancer cell lines have previously been shown to be more sensitive, in general, to solid tumor cell lines²⁸. In addition, certain hematological tumor types show exquisite sensitivity to PBD dimers which may predict target ADC cytotoxicity independently of CD19 expression above a threshold expression level. It has previously been shown that, for example, defects in homologous recombination repair or DNA repair protein ERCC1 confer increased sensitivity to PBD dimers²⁹ suggesting a possible widening of therapeutic index in patients with tumors harbouring these defects, and indicates potential biomarkers of response.

Evidence of rapid internalization of ADCT-402 is provided by the reduction in intensity of membrane immunofluorescence staining on CD19-expressing Ramos cells. Co-localization images suggest that processing of ADCT-402 is, at least in part, lysosomal. The time lag observed between the peak of DNA interstrand cross-link formation by ADCT-402 and by the naked warhead SG3199 reflects the time taken for internalization and cellular processing of the ADC compared with the readily diffusible PBD dimer. An important feature of the

highly cytotoxic cross-links produced is the minimal distortion of DNA which contribute to the lack of repair and consequent persistence over a 36-h period observed.

If ADCT-402 is to be efficacious in lymphomas with heterogeneous CD19 expression, the existence of bystander toxicity of target-negative tumor cells is important. PBD warhead released from the target-positive cell would be expected to be diffusible in contrast to less permeable payloads such as MMAF. In medium transfer experiments, CD19-negative Karpas-299 cells were killed by a soluble factor released from ADCT-402-treated Ramos cells into the medium. This soluble factor is assumed to be SG3199 warhead, released by lysosomal cleavage of the val-ala dipeptide linker in ADCT-402 and the self-immolative cleavage of the residual linker stub on the PBD N10 imine, since we have shown that any transfer of intact ADC would be inactive against the CD19-negative cells.

In vivo efficacy experiments show remarkable dose-related improvements in survival in both s.c. and disseminated models in three different tumor types (Burkitt's lymphoma, ALL and DLBCL). Clear superiority is observed compared to comparator ADCs delivering tubulin inhibitor drugs, reflecting the increased potency of the PBD dimer warhead and the inherent sensitivity of haematological malignancies to critical DNA damage. It is clear that a single dose of ADCT-402 can selectively deliver sufficient cytotoxic agent, not only to induce growth delay, but also sustained tumor regression and in many cases tumor eradication. Interestingly, in the Ramos model, peak drug concentration (C_{max}) appears to be necessary for complete response since administering the same total dose fractionated into three administrations (over two weeks or eight days) was significantly inferior, producing only tumor growth delay. This is in contrast to a recent report which observed similar anti-tumor activity against solid tumor xenografts in mice treated with single or fractionated dosing³⁰.

Anti-PBD payload antibody and anti- γ -H2AX staining confirmed the dose-dependent delivery of ADCT-402 to the target tumor xenograft. In addition, quantitative pharmacodynamic assessment of DNA cross-linking and γ -H2AX foci containing cells was achieved. γ -H2AX

has previously been shown to be a highly sensitive DNA damage response marker to DNA cross-linking agents including PBD dimers^{31,32}, and both γ -H2AX immunofluorescence and measurement of DNA interstrand cross-links by comet assay have been used as pharmacodynamic assays in clinical trials of PBD dimer SG2000^{17,32}. Extrapolating from the *in vivo* data suggests that a threshold level of DNA interstrand cross-linking is required for tumor regression and eradication. This is consistent with previous data with CD25-targeting ADCT-301¹⁵ and also with the inferior fractionated dosing observed in this study. The absence of DNA cross-linking in mouse PBMCs supports the specificity of ADCT-402 *in vivo*.

No change in expression of CD19 was observed in tumors 24 h post ADCT-402 administration *in vivo*. An important consideration in the design of early phase clinical studies of ADCT-402 is the level and heterogeneity of target CD19 expression in patient tumors in the relevant R/R setting. To address this, we examined CD19 expression in a panel of matched (initial diagnosis and R/R) clinical samples (Table 1). High and homogeneous CD19 expression was observed across the whole panel of matched samples confirming maintenance of target antigen expression from initial diagnosis to relapse and confirming the excellent widespread nature of CD19 as an ideal target for clinical ADC development.

ADCT-402 was found to have a favourable safety and PK profile with excellent stability in both rat and cynomolgus monkey. Taken together, these impressive pre-clinical data were used to support the rapid clinical testing of ADCT-402 in patients with CD19-expressing B-cell malignancies. Phase I studies in both R/R NHL and R/R B-ALL are currently underway. Emerging clinical data confirm the potential of this therapy in targeting CD19-expressing B-cell malignancies³³⁻³⁵.

Acknowledgements:

The authors thank Charles River Laboratory Services, Epo-GmbH and Covance for conducting the *in vivo* studies, and PRA Health Services for the PK measurements. Animal studies conducted at EPO GmbH were approved by LaGeSo (A0452/8). J.A. Hartley acknowledges Programme Grant support from Cancer Research UK (C2559A/A16569). This work was also supported by grants from the UCLH/UCL NIHR Comprehensive Biomedical Research Centre (TM).

Authorship contributions:

F.Z. designed experiments, interpreted data, prepared figures and wrote the paper. S.Co., L.A., P.C.T., K.K., N.J., C.E.B., F.D'H. designed and performed experiments; T.M., C.E.G.H., S.Ch., D.G.W. designed experiments and interpreted data. A.T. and P.W.H. provided guidance on PBD chemistry; J.A.H designed experiments, interpreted data and wrote the paper; P.H.B. interpreted data, provided guidance and intellectual input.

Conflict of Interest Disclosure:

F.Z., C.E.B., C.E.G.H., S.C. and P.H.B. are employees of ADC Therapeutics and P.H.B., J.A.H. and P.W.H. are also major shareholders. L.A., P.C.T., D.G.W., A.T., P.W.H. and J.A.H. are employees of Spirogen/Medimmune limited. The current affiliation of F.D'H. is Novasep, Le Mans, France.

Correspondence:

Francesca Zammarchi, ADC Therapeutics (UK) Limited, QMB Innovation Centre, 42 New Road, London, E1 2AX, UK; e-mail: francesca.zammarchi@adctherapeutics.com.

REFERENCES

1. Tedder TF. CD19: a promising B cell target for rheumatoid arthritis. *Nat Rev Rheumatol*. 2009;5(10):572-577.
2. Haas KM, Tedder TF. Role of the CD19 and CD21/35 receptor complex in innate immunity, host defense and autoimmunity. *Adv Exp Med Biol*. 2005;560:125-139.
3. Wang K, Wei G, Liu D. CD19: a biomarker for B cell development, lymphoma diagnosis and therapy. *Exp Hematol Oncol*. 2012;1(1):36.
4. Scheuermann RH, Racila E. CD19 antigen in leukemia and lymphoma diagnosis and immunotherapy. *Leuk Lymphoma*. 1995;18(5-6):385-397.
5. Jabbour E, O'Brien S, Ravandi F, Kantarjian H. Monoclonal antibodies in acute lymphoblastic leukemia. *Blood*. 2015;125(26):4010-4016.
6. Kantarjian H, Stein A, Gokbuget N, et al. Blinatumomab versus Chemotherapy for Advanced Acute Lymphoblastic Leukemia. *N Engl J Med*. 2017;376(9):836-847.
7. Lee DW, Kochenderfer JN, Stetler-Stevenson M, et al. T cells expressing CD19 chimeric antigen receptors for acute lymphoblastic leukaemia in children and young adults: a phase 1 dose-escalation trial. *Lancet*. 2015;385(9967):517-528.
8. Gerber HP, Kung-Sutherland M, Stone I, et al. Potent antitumor activity of the anti-CD19 auristatin antibody drug conjugate hBU12-vcMMAE against rituximab-sensitive and -resistant lymphomas. *Blood*. 2009;113(18):4352-4361.
9. Blanc V, Bousseau A, Caron A, Carrez C, Lutz RJ, Lambert JM. SAR3419: an anti-CD19-Maytansinoid Immunoconjugate for the treatment of B-cell malignancies. *Clin Cancer Res*. 2011;17(20):6448-6458.
10. Cooper LJ, Al-Kadhimi Z, DiGiusto D, et al. Development and application of CD19-specific T cells for adoptive immunotherapy of B cell malignancies. *Blood Cells Mol Dis*. 2004;33(1):83-89.
11. Moskowitz CH, Fanale MA, Shah BD, et al. A Phase 1 Study of Denintuzumab Mafodotin (SGN-CD19A) in Relapsed/Refractory B-Lineage Non-Hodgkin Lymphoma. *Blood*. 2015;126(23):Abstract 182.
12. Coiffier B, Thieblemont C, de Guibert S, et al. A phase II, single-arm, multicentre study of coltuximab ravtansine (SAR3419) and rituximab in patients with relapsed or refractory diffuse large B-cell lymphoma. *Br J Haematol*. 2016;173(5):722-730.
13. Kung Sutherland MS, Walter RB, Jeffrey SC, et al. SGN-CD33A: a novel CD33-targeting antibody-drug conjugate using a pyrrolobenzodiazepine dimer is active in models of drug-resistant AML. *Blood*. 2013;122(8):1455-1463.
14. Saunders LR, Bankovich AJ, Anderson WC, et al. A DLL3-targeted antibody-drug conjugate eradicates high-grade pulmonary neuroendocrine tumor-initiating cells in vivo. *Sci Transl Med*. 2015;7(302):302ra136.
15. Flynn MJ, Zammarchi F, Tyrer PC, et al. ADCT-301, a Pyrrolobenzodiazepine (PBD) Dimer-Containing Antibody-Drug Conjugate (ADC) Targeting CD25-Expressing Hematological Malignancies. *Mol Cancer Ther*. 2016;15(11):2709-2721.
16. Hartley JA. The development of pyrrolobenzodiazepines as antitumour agents. *Expert Opin Investig Drugs*. 2011;20(6):733-744.
17. Puzanov I, Lee W, Chen AP, et al. Phase I pharmacokinetic and pharmacodynamic study of SJG-136, a novel DNA sequence selective minor groove cross-linking agent, in advanced solid tumors. *Clin Cancer Res*. 2011;17(11):3794-3802.
18. Janjigian YY, Lee W, Kris MG, et al. A phase I trial of SJG-136 (NSC#694501) in advanced solid tumors. *Cancer Chemother Pharmacol*. 2010;65(5):833-838.
19. Hartley JA, Flynn MJ, Bingham JP, et al. Pre-clinical pharmacology and mechanism of action of SG3199, the pyrrolobenzodiazepine (PBD) dimer warhead component of antibody-drug conjugate (ADC) payload tesirine. *In preparation*.

20. Tiberghien AC, Levy JN, Masterson LA, et al. Design and Synthesis of Tesirine, a Clinical Antibody-Drug Conjugate Pyrrolobenzodiazepine Dimer Payload. *ACS Med Chem Lett.* 2016;7(11):983-987.
21. Rudin CM, Pietanza MC, Bauer TM, et al. Rovalpituzumab tesirine, a DLL3-targeted antibody-drug conjugate, in recurrent small-cell lung cancer: a first-in-human, first-in-class, open-label, phase 1 study. *Lancet Oncol.* 2017;18(1):42-51.
22. Al-Katib AM, Aboukameel A, Mohammad R, Bissery MC, Zuany-Amorim C. Superior antitumor activity of SAR3419 to rituximab in xenograft models for non-Hodgkin's lymphoma. *Clin Cancer Res.* 2009;15(12):4038-4045.
23. Spanswick VJ, Hartley JM, Hartley JA. Measurement of DNA interstrand crosslinking in individual cells using the Single Cell Gel Electrophoresis (Comet) assay. *Methods Mol Biol.* 2010;613:267-282.
24. Swerdlow SH, Campo E, Pileri SA, et al. The 2016 revision of the World Health Organization classification of lymphoid neoplasms. *Blood.* 2016;127(20):2375-2390.
25. Roguska MA, Pedersen JT, Henry AH, et al. A comparison of two murine monoclonal antibodies humanized by CDR-grafting and variable domain resurfacing. *Protein Eng.* 1996;9(10):895-904.
26. Zein N, Sinha AM, McGahren WJ, Ellestad GA. Calicheamicin gamma 1I: an antitumor antibiotic that cleaves double-stranded DNA site specifically. *Science.* 1988;240(4856):1198-1201.
27. Ryan MC, Palanca-Wessels MC, Schimpf B, et al. Therapeutic potential of SGN-CD19B, a PBD-based anti-CD19 drug conjugate, for treatment of B-cell malignancies. *Blood.* 2017.
28. Hartley JA, Spanswick VJ, Brooks N, et al. SJG-136 (NSC 694501), a novel rationally designed DNA minor groove interstrand cross-linking agent with potent and broad spectrum antitumor activity: part 1: cellular pharmacology, in vitro and initial in vivo antitumor activity. *Cancer Res.* 2004;64(18):6693-6699.
29. Clingen PH, De Silva IU, McHugh PJ, et al. The XPF-ERCC1 endonuclease and homologous recombination contribute to the repair of minor groove DNA interstrand crosslinks in mammalian cells produced by the pyrrolo[2,1-c][1,4]benzodiazepine dimer SJG-136. *Nucleic Acids Res.* 2005;33(10):3283-3291.
30. Hinrichs MJM, Ryan PM, Zheng B, et al. Fractionated Dosing Improves Preclinical Therapeutic Index of Pyrrolobenzodiazepine-Containing Antibody Drug Conjugates. *Clin Cancer Res.* 2017.
31. Clingen PH, Wu JY, Miller J, et al. Histone H2AX phosphorylation as a molecular pharmacological marker for DNA interstrand crosslink cancer chemotherapy. *Biochem Pharmacol.* 2008;76(1):19-27.
32. Wu J, Clingen PH, Spanswick VJ, et al. gamma-H2AX foci formation as a pharmacodynamic marker of DNA damage produced by DNA cross-linking agents: results from 2 phase I clinical trials of SJG-136 (SG2000). *Clin Cancer Res.* 2013;19(3):721-730.
33. Kahl B.S., Hamadani M. , Caimi P. F. , et al. First Clinical Results of ADCT-402, a Novel Pyrrolobenzodiazepine-Based Antibody Drug Conjugate (ADC), in Relapsed/Refractory B-cell Lineage NHL. *Hematological Oncology.* 2017;35(S2).
34. Kahl B, Hamadani M, Caimi P, et al. Encouraging Early Results from the First-In-Human Clinical Trial of ADCT-402 (Loncastuximab Tesirine), a Novel Pyrrolobenzodiazepine-Based Antibody Drug Conjugate, in Relapsed/Refractory B-Cell Lineage Non-Hodgkin Lymphoma. *59th ASH Annual Meeting.* 2017.
35. Jain N, Klisovic R, Stock W, et al. Interim Data from a Phase 1 Study Evaluating Pyrrolobenzodiazepine-Based Antibody Drug Conjugate ADCT-402 (Loncastuximab Tesirine) Targeting CD19 for Relapsed or Refractory B-Cell Acute Lymphoblastic Leukemia. *59th ASH Annual Meeting.* 2017.

Table 1. CD19 expression in matched primary and relapsed clinical samples

Clinical subtype	Case no. Primary(P)/ Relapsed (R)	Biopsy type	Time between biopsy (months)	CD19 ^{a,b} intensity
Diffuse Large B cell Lymphoma	1P 1R	BM BM	8	2 3
	2P 2R	LN mesenteric mass	20	3 3
	3P 3R	testis penile mass	12	3 3
	4P 4R	LN LN	14	3 3
	5P 5R	BM LN	8	2 3
Mantle Cell Lymphoma	6P 6R	salivary gland submandibular	20	3 3
	7P 7R	BM LN	11	3 3
	8P 8R	LN LN	15	3 3
	9P 9R	gastrointestinal duodenal bulb	8	3 3
Follicular Lymphoma	10P 10R	LN LN	27	3 3
	11P 11R	LN LN	26	3 3
Small Lymphocytic Lymphoma/Chronic Lymphocytic Leukemia	12P 12R	BM BM	20	3 2

BM, bone marrow; LN, lymph node

^a 0 = negative, 1 = weak, 2 = moderate, 3 = strong staining as determined by pathologist review

^b In all samples analysed, >80% tumor cells were CD19 +ve

FIGURE LEGENDS

Figure 1. Characterization of ADCT-402. A. Structure of ADCT-402. B. ADCT-402 characterised by size exclusion chromatography (SEC). C. Reduced reverse phase liquid chromatography (RPLC) depicting reduced heavy and light chains of ADCT-402. D. Hydrophobic interaction chromatography (HIC) depicting DAR forms of ADCT-402.

Figure 2. Correlation between *in vitro* cytotoxicity and cell surface CD19 density. A. IC₅₀ values (mean of three independent determinations) of ADCT-402 against the named cell lines are plotted against the measured cell surface CD19 levels expressed as sites/cell. The line is the regression through all data points. B. The equivalent analysis performed for the naked PBD dimer warhead SG3199. Linear relationship between indicated variables was calculated by Pearson correlation coefficient *r* test.

Figure 3. Mechanism of action of ADCT-402. A. Merged immunofluorescent images of CD19-positive, human Burkitt's lymphoma-derived Ramos cells treated with 2 µg/ml ADCT-402 for 1 h, washed and fixed after T=0, 1, 2, 4 or 24 h in medium at 37°C and stained with labelled anti-human IgG (green), anti-LAMP-1 (red) and Hoechst 33342 (blue) nuclear stain. Yellow indicates co-localization, with specific sites of co-localization indicated by stars. B. Time course of DNA interstrand cross-linking measured as the % reduction on Olive Tail Moment (OTM) in Ramos cells treated for 2 h with ADCT-402 (40 pM), SG3199 (10 pM) or a non-targeted ADC (40 pM) followed post-incubation in drug-free medium for the indicated time. Results are the mean ± s.d. from at least three independent experiments. C. Percentage viability of CD19-negative Karpas-299 cells after 96 h exposure to media transferred from ADCT-402-treated CD19-positive Ramos cells or CD19-negative NCI-N87 cells for 1, 2 or 3 days. Statistical analysis was done with unpaired *t* test with Welch's

correction (not assuming equal SD's). The p values are two-tailed, * = $p \leq 0.05$, ** = $p \leq 0.01$; ns = not significant.

Figure 4. Comparative anti-tumor activity of ADCT-402 in the human CD19-expressing Burkitt's lymphoma-derived Ramos model. A. In vivo anti-tumor activity of ADCT-402 in s.c. implanted Ramos xenograft model. ADCT-402 was administered IV at a group mean tumor volume of 120 mm^3 as a single dose at 0.33, 0.66 or 1 mg/kg. B. In vivo anti-tumor activity of ADCT-402 in s.c. implanted Ramos xenograft model in comparison to ADCs RB4v1.2-DM4 and hBU12-mc-MMAF. All three ADCs were compared at a single dose of 1 mg/kg and in addition RB4v1.2-DM4 and hBU12-mc-MMAF were also tested at 3.3 mg/kg, q4d x 2 and 3 mg/kg, q4d x 4, respectively. C. In vivo anti-tumor activity of ADCT-402 in s.c. implanted Ramos xenograft model where ADCT-402 was administered at a single dose of 1 mg/kg or fractionated dosing of 0.33 mg/kg given either qwk x 3 or q4d x 3. Data in panels A-C are shown as mean \pm standard error of the mean (SEM) from animal group sizes of 10 mice. D. *In vivo* anti-tumor activity of ADCT-402 in a disseminated Ramos model. Kaplan-Meier survival plots show percentage animal survival over 91 days in an experiment in which ADCT-402 was administered at a single dose of 0.33 mg/kg or 1 mg/kg in comparison to vehicle or non-targeting ADC administered as a single dose of 1 mg/kg (each group n = 10).

Figure 5. Anti-tumor activity of ADCT-402 in a range of tumor models. A. In vivo anti-tumor activity of ADCT-402 in s.c. implanted CD19-expressing Burkitt's lymphoma-derived Daudi xenograft model. ADCT-402 was administered IV at a group mean tumor volume of 130 mm^3 as a single dose at 0.1 mg/kg or 0.3 mg/kg. B. In vivo anti-tumor activity of ADCT-402 in s.c. implanted CD19-expressing diffuse-large B-cell lymphoma-derived WSU-DLCL2 xenograft model. ADCT-402 was administered IV at a group mean tumor volume of 120 mm^3 as a single dose at 0.3 mg/kg or 1 mg/kg. Data in panels A and B are the mean \pm SEM from animal group sizes of 10 mice. C. In vivo anti-tumor activity of ADCT-402 in a disseminated CD19-expressing acute-lymphoblastic leukemia-derived NALM-6 model. Kaplan-Meier

survival plots show percentage animal survival over 90 days in an experiment in which ADCT-402 was administered at a single dose of 0.33 mg/kg or 1 mg/kg in comparison to vehicle or non-targeting ADC administered as a single dose of 1 mg/kg (each group n = 10).

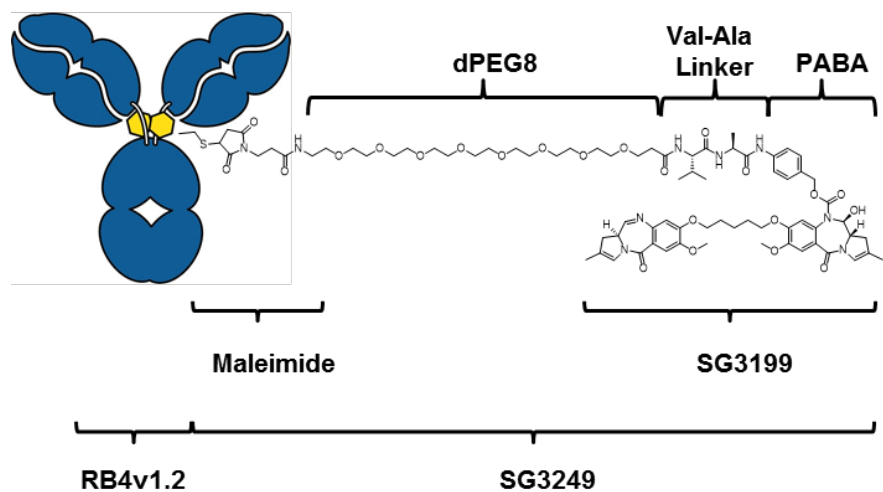
Figure 6. Pharmacodynamic studies of ADCT-402. A. Representative scans of formalin fixed paraffin embedded (FFPE) Ramos xenograft tumor sections, obtained from vehicle-treated control mice or mice treated with 0.3 mg/kg and 1 mg/kg ADCT-402 or 1 mg/kg non-targeting ADC and stained with an anti-CD19 antibody (top panels), anti-PBD linker antibody (middle panels) or an anti- γ -H2AX antibody (bottom panels). B. Histogram depicting % cells with γ -H2AX in tumor cell suspensions taken from Ramos xenograft tumors 24 h after injection with vehicle or 0.3 mg/kg or 1 mg/kg ADCT-402 or 1 mg/kg non-targeted ADC. Data represent the mean and standard deviation (SD) from three individual mice per data point. ** = $p \leq 0.01$, *** = $p \leq 0.001$, ns = non-significant. C. Histogram depicting mean OTM in irradiated (I) or unirradiated (UI) tumor cell suspensions taken from Ramos xenograft tumors 24 h after injection with vehicle or 0.3 mg/kg or 1 mg/kg ADCT-402 or 1 mg/kg non-targeted ADC. Data represent the mean and SD from three individual mice per data point. Statistical analysis was done with unpaired t-Test with Welch's correction (not assuming equal SD's). The P values are two-tailed; * = $p \leq 0.05$, ** = $p \leq 0.01$.

Figure 7. Pharmacokinetics of ADCT-402 in rat and cynomolgus monkey. A.

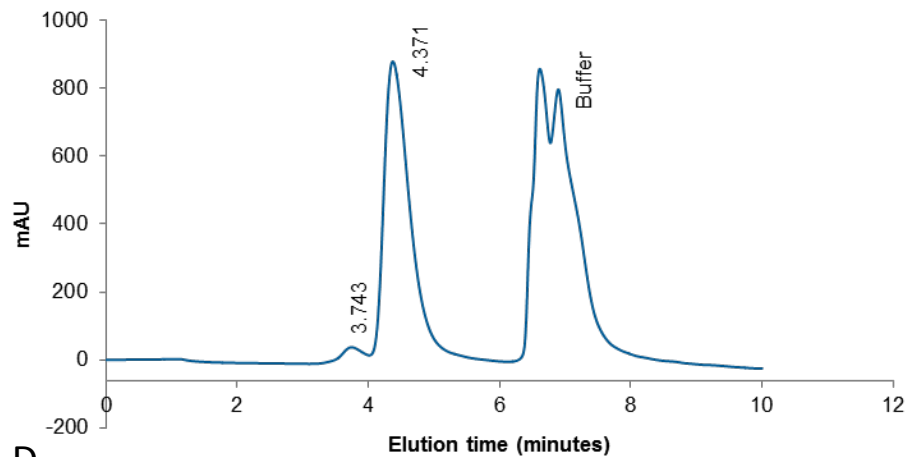
Quantitation of total antibody and PBD-conjugated ADCT-402 in rat serum from three individual Crl:CD(SD) rats treated with a single IV dose of 1.5 mg/kg. B. Quantitation of total antibody, PBD-conjugated antibody and free PBD dimer warhead SG3199 in cynomolgus monkey serum after IV administration of 0.6 mg/kg ADCT-402 on days 1 and 22. The results are mean \pm SEM (n=2/5 male and 2/5 female).

Figure 1

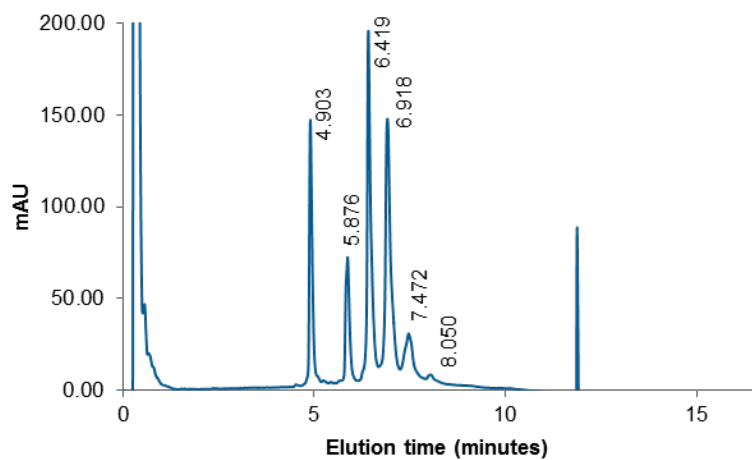
A



B



C



D

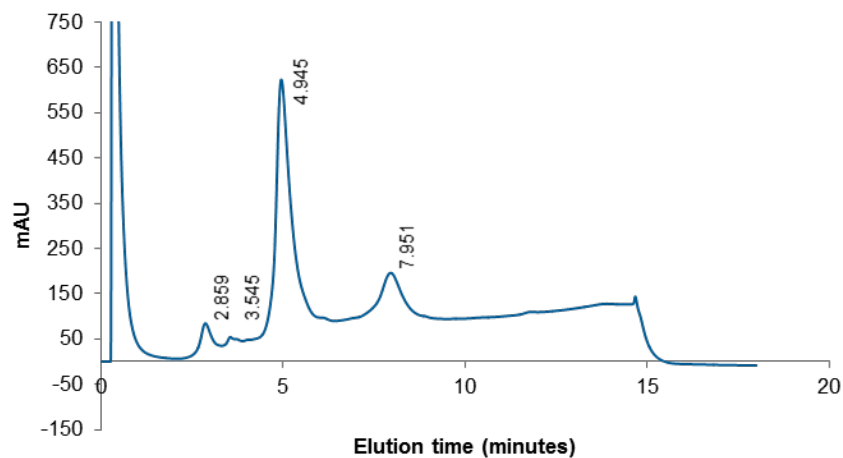
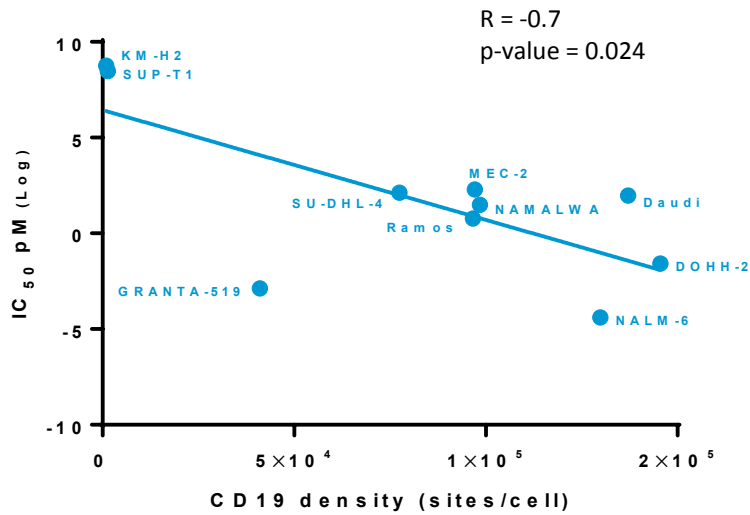


Figure 2

A



B

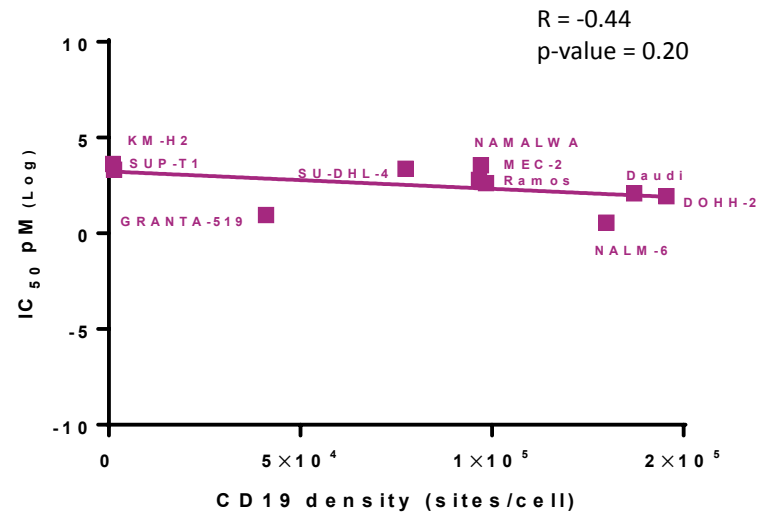


Figure 3

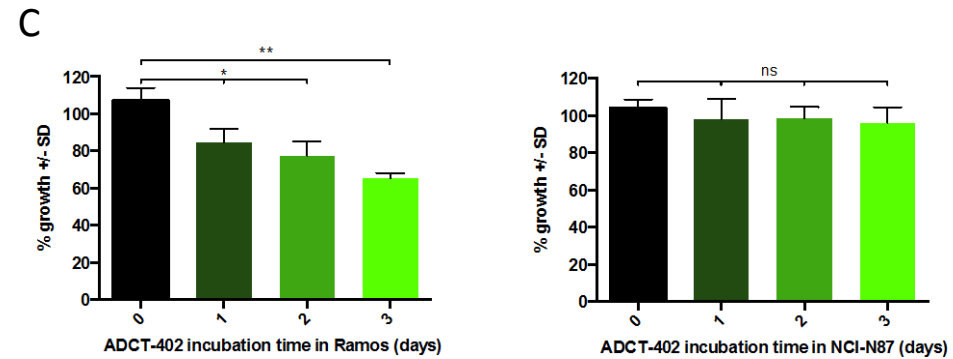
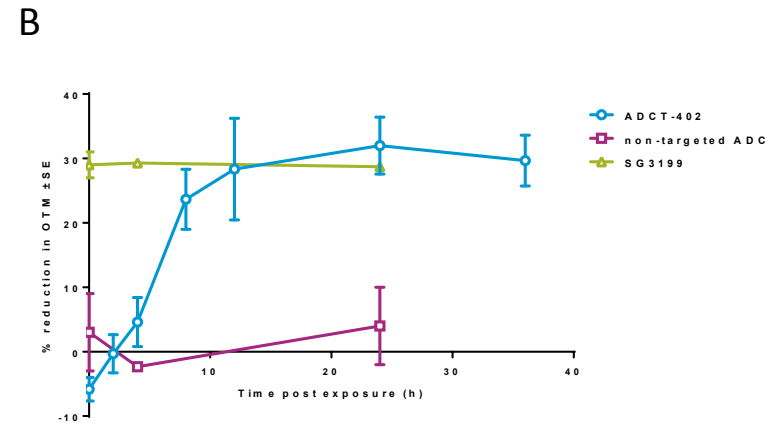
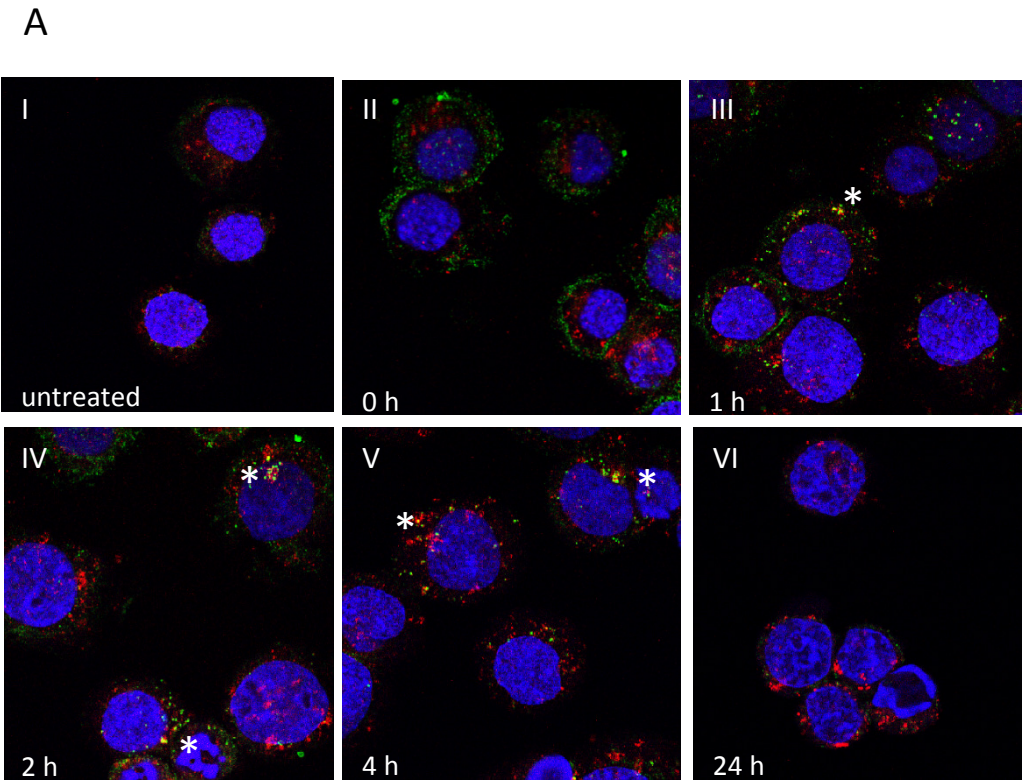
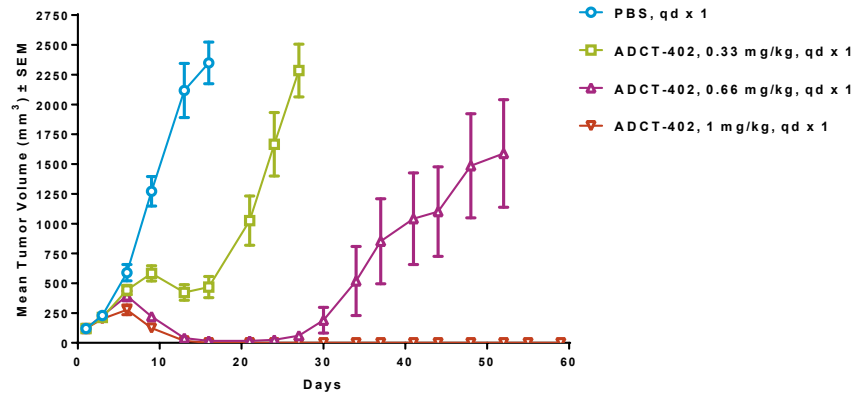
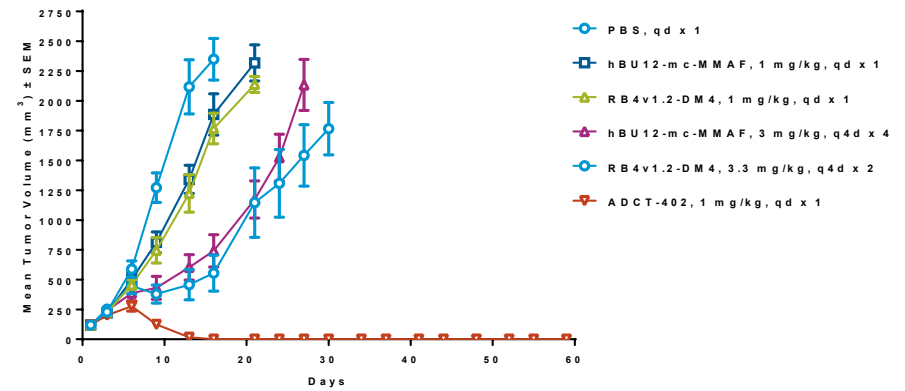


Figure 4

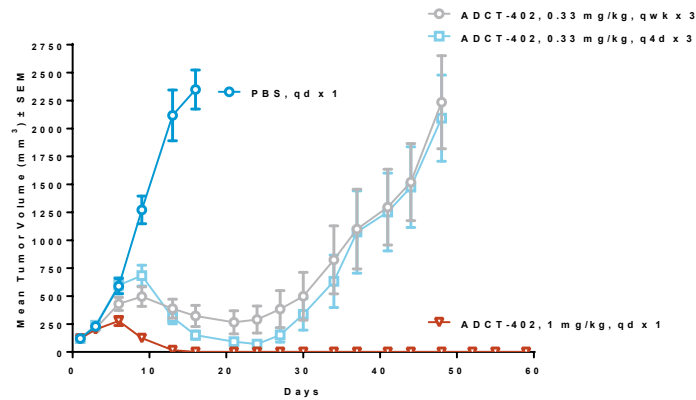
A



B



C



D

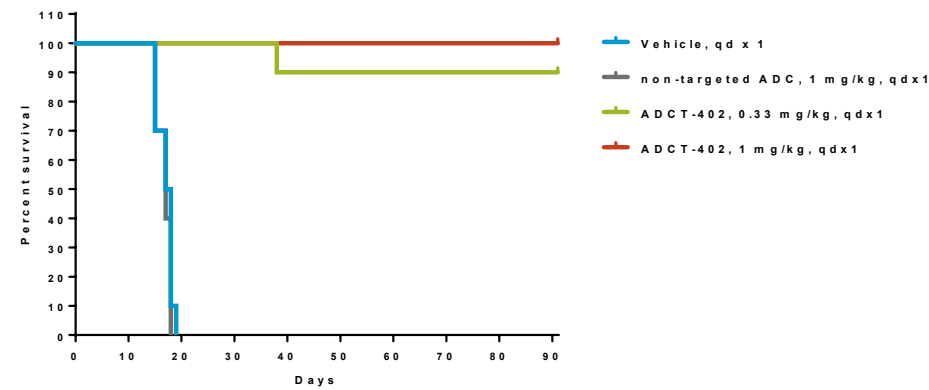
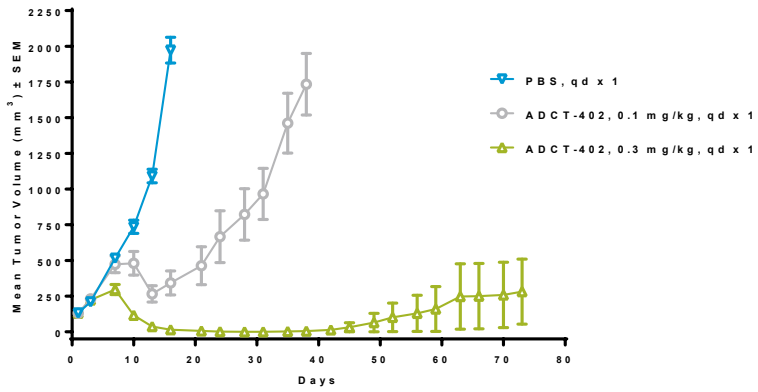
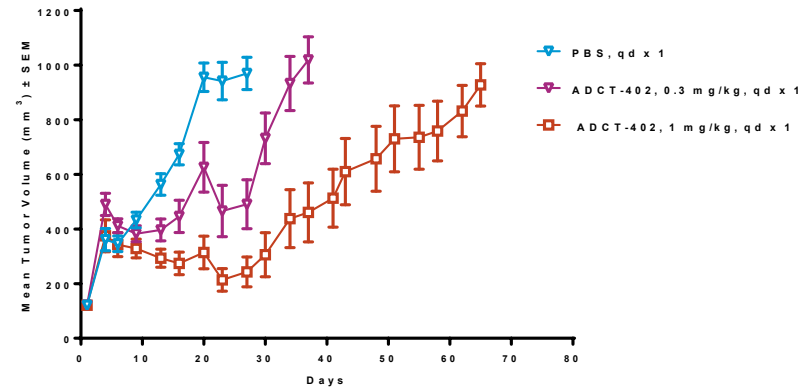


Figure 5

A



B



C

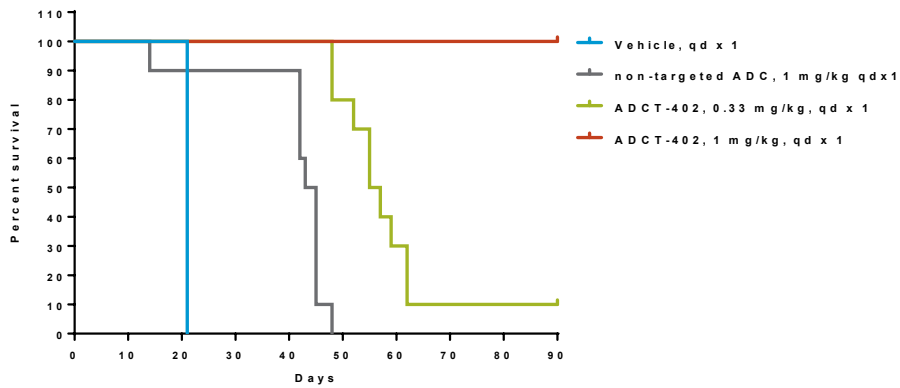


Figure 6

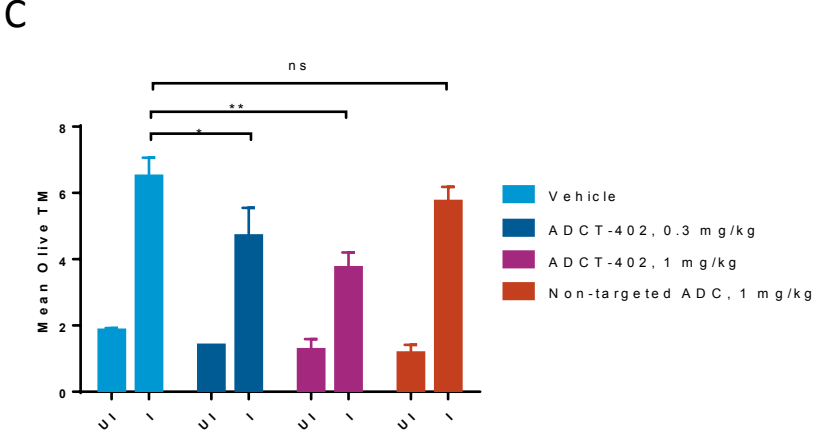
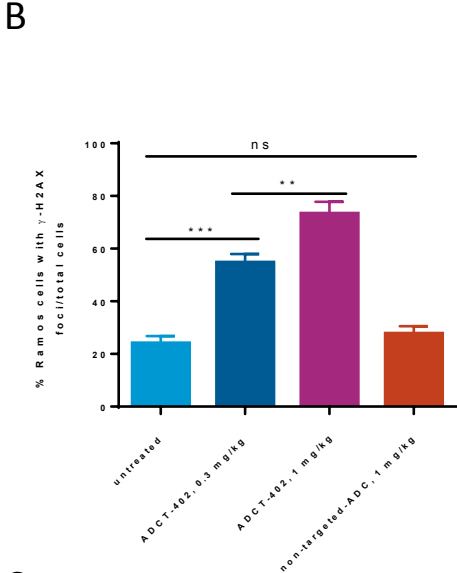
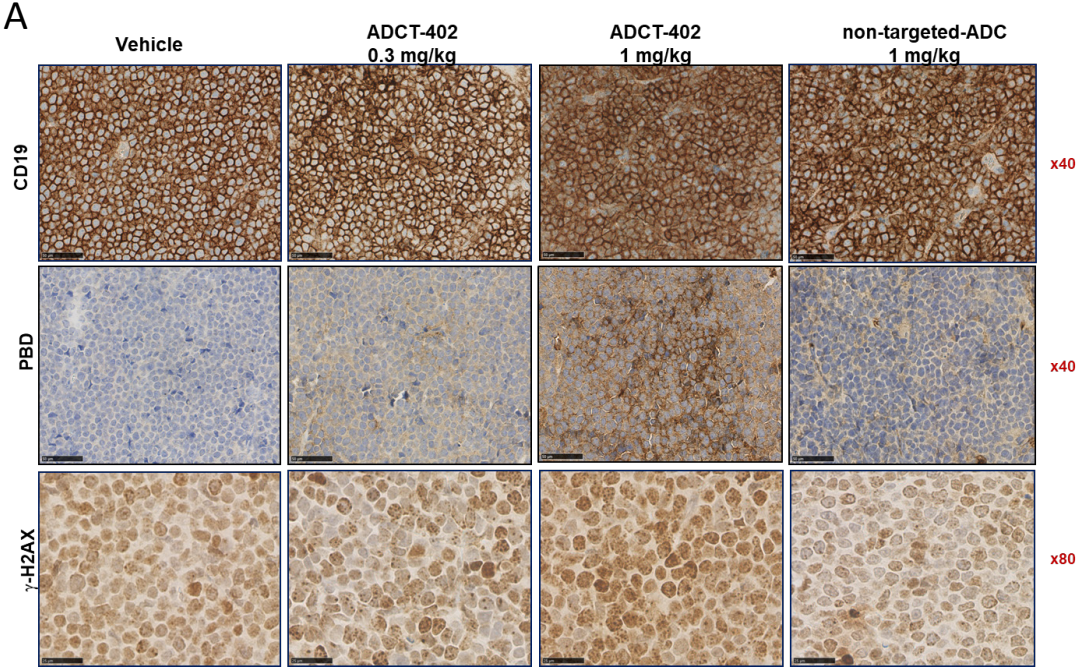
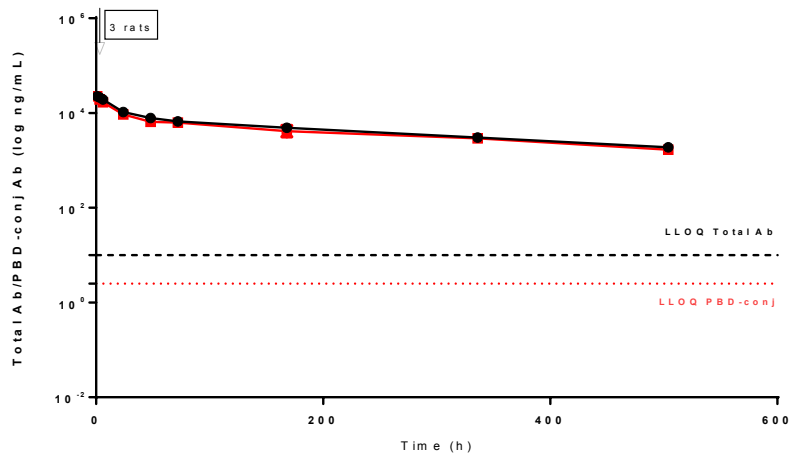


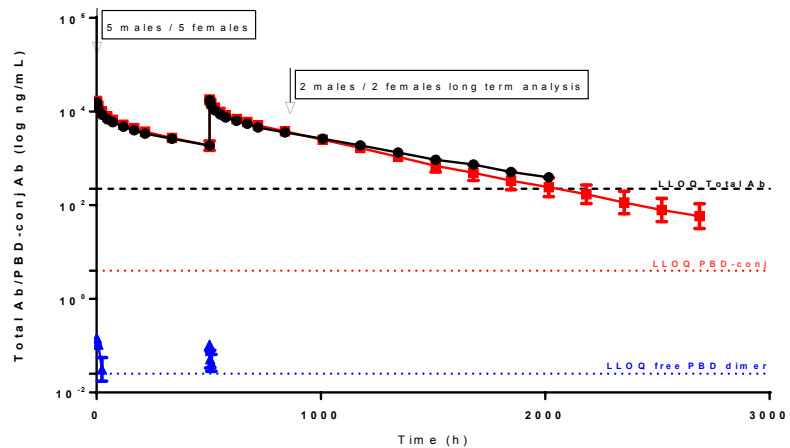
Figure 7

A



● Total conjugated antibody (DAR ≥ 1)
■ Total antibody (DAR > 0)

B



● Total antibody (DAR ≥ 0)
■ Total conjugated antibody (DAR ≥ 1)
▲ free PBD dimer



blood[®]

Prepublished online January 3, 2018;
doi:10.1182/blood-2017-10-813493

ADCT-402, a PBD dimer-containing antibody drug conjugate targeting CD19-expressing malignancies

Francesca Zammarchi, Simon Corbett, Lauren Adams, Peter C. Tyrer, Konstantinos Kiakos, Narinder Janghra, Teresa Marafioti, Charles E. Britten, Carin E.G. Havenith, Simon Chivers, Francois D'Hooge, David G. Williams, Arnaud Tiberghien, Philip W. Howard, John A Hartley and Patrick H. van Berkel

Information about reproducing this article in parts or in its entirety may be found online at:
http://www.bloodjournal.org/site/misc/rights.xhtml#repub_requests

Information about ordering reprints may be found online at:
<http://www.bloodjournal.org/site/misc/rights.xhtml#reprints>

Information about subscriptions and ASH membership may be found online at:
<http://www.bloodjournal.org/site/subscriptions/index.xhtml>

Advance online articles have been peer reviewed and accepted for publication but have not yet appeared in the paper journal (edited, typeset versions may be posted when available prior to final publication). Advance online articles are citable and establish publication priority; they are indexed by PubMed from initial publication. Citations to Advance online articles must include digital object identifier (DOIs) and date of initial publication.